Journal of Solid State Chemistry 181 (2008) 2719–2724

Contents lists available at ScienceDirect

Journal of Solid State Chemistry

journal homepage: www.elsevier.com/locate/jssc

Crystal structure and high-pressure studies of WAl_2, an aluminide crystallizing with the $CrSi_2$ structure type

Q.F. Gu, D.Y. Jung, G. Krauss *, W. Steurer

Laboratory of Crystallography, Department of Materials, ETH, Zurich 8093, Switzerland

ARTICLE INFO

Article history:
Received 29 April 2008
Received in revised form
25 June 2008
Accepted 26 June 2008
Available online 2 July 2008

Keywords:
Diamond-anvil cell
High pressure
ELF
Intermetallic compound

ABSTRACT

The novel intermetallic compound WAl_2 crystallizes with space group $P6_422$ and lattice parameters $a = 4.7422(1)$ Å, $c = 6.6057(2)$ Å. The crystal structure was solved from single-crystal X-ray diffraction data. WAl_2 was found to be the first aluminide that is isotypic with $CrSi_2$. A high-pressure powder X-ray diffraction study showed its stability up to at least 31.5(1) GPa. The bulk modulus was calculated by fitting a third-order Birch–Murnaghan equation of state to the pressure–volume data as $K_0 = 168(11)$ GPa and its pressure derivative $K' = 7.7(1.0)$. Partially covalent bonding between W and Al atoms was indicated by means of the electron localization function (ELF) and explains the anisotropic compression behavior. Quantum chemical calculations identify WAl_2 as a potential high-temperature phase.

1. Introduction

Recently, complex metallic alloys (CMAs) attracted more and more attention due to their potential unusual physical properties caused by different length scales present in their structures [1]. Within our recent studies on the structures, stability, and compressibility of CMAs [2–4], the system W–Al was subject of investigation. According to the literature data, the binary system W–Al has still open questions. Three intermetallic compounds are characterized, i.e. WAl_4 [5], WAl_5 [6], and WAl_{12} [7]. Three additional phases, WAl_3 (ζ-phase), W_3Al_7 (η-phase), and W_7Al_{13} (θ-phase), are proposed as high-temperature phases, being stable above at least 1302 °C [8]. Up to now, the complexity of intermetallic compounds cannot be predicted and in some case, compounds with a high structural complexity show a quite simple composition, like e.g. β-Mg_2Al_3 [9]. These facts gave us the motivation to reinvestigate the W–Al binary system at compositions around W:Al = 1:2. We report here on synthesis, crystal structure, chemical bonding analysis, and high-pressure studies on the novel intermetallic compound WAl_2.

2. Experimental section

Starting materials for preparation of WAl_2 were high-purity elements: W (99.995% powder, Alfa Aesar), and Al (99.95% wire, Alfa Aesar). W powder, pressed into a pellet in an argon-filled glove box and Al in molar ratio of W:Al = 1:3 was carefully melted in an arc furnace under argon atmosphere several times for homogenization. The ingot was annealed at 1000 °C for 2 weeks in an alumina crucible sealed in a quartz ampoule, and subsequently quenched in water. The phase composition was studied using a STOE stadi-P powder diffractometer and Co$K\alpha_1$ radiation. Two synthesis products were identified, i.e. WAl_4 and WAl_2. The two phases were distinguishable due to their different crystal morphologies: WAl_4 forms thin plate like, WAl_2 hexagonal columnar crystals. The chemical composition of several single crystals of WAl_2 was determined by energy dispersive X-ray analysis (EDX, LEO 1530) to 67.3(2.2) at% Al and 32.7(1.5) at% W (calculated: W 66.6 at%, Al 33.3 at%). There were no other elements found in detectable amounts. Differential thermal analysis (DTA) measurements were done on a Perkin-Elmer DTA7 system in the range of 400–1500 °C using alumina crucibles in Ar-atmosphere and heating and cooling rates of 10 K/min. Single-crystal X-ray diffraction data were collected on an Oxford Diffraction XCalibur XP diffractometer equipped with an Onyx CCD-detector using Mo$K\alpha$ radiation (Oxford Enhance). Indexing, data reduction, and numerical absorption correction of measured data were performed by the use of the CrysAlis RED program package [10]. Crystal structures were solved by using ShelXS [11] and structure models refined against F^2 using the ShelXL97 program [11].

High-pressure X-ray diffraction was performed with an in-house rotating-anode generator using a Mo target and Johansson monochromator (Mo$K\alpha_1$ radiation). The two-dimensional (2D) diffraction data were collected on a Marresearch mar300 IP-detector. High pressures up to 31.5(2) GPa at ambient temperature were generated by use of the ETH diamond-anvil cell (DAC) and a

* Corresponding author. Fax: +41 44 632 11 33.
E-mail address: guenter.krauss@mat.ethz.ch (G. Krauss).

0022-4596/$ - see front matter © 2008 Elsevier Inc. All rights reserved.
doi:10.1016/j.jssc.2008.06.053

tungsten gasket. The pressure-induced fluorescence shift of ruby was used for pressure determination. WAl_2 single crystals were selected from the ingot and ground in an agate mortar for the HP powder diffraction experiments. The phase purity of the obtained powder was checked by X-ray diffraction. A mixture of methanol, ethanol and water (16:3:1) served as pressure-transmitting medium, which constituted about one third of the total volume of the sample chamber (70% sample) to minimize deviatoric stress. To minimize the unwanted scattering of the gasket, the beam diameter was reduced by slits to about $200 \times 200\,\mu m^2$. Integration of the 2D powder pattern was realized by means of the program fit 2D [12], and one-dimensional (1D) powder pattern were refined by applying the Rietveld method using the program GSAS [13]. Equations of state were calculated by the use of the program EosFit5.2 [14].

2.1. Quantum chemical calculations

Present calculations have been performed with the Vienna *ab initio* simulation package (VASP) [15,16] code. The generalized gradient approximation (GGA) [17] together with the projector augmented wave (PAW) [18] method have been used to calculate energies of the different structures at 0 K. In all calculations, the following PAW potentials were used: Core region cut-off are 2.5 atomic units (a.u.[1]) (core configuration $[Xe]4d^{10}5s^24f^{14}$ and 1.9 a.u. for aluminum (core configuration $1s^22s^22p^6$). A plane wave cut-off energy of 600 eV[2] for all structures proved to be reliable (convergence of energy to within 1.5×10^{-4} eV/atom, convergence of pressure to within 0.02 GPa) and computationally acceptable. The energy differences converge to within 1×10^{-4} eV/atom. For the Brillouin zone sampling the Monkhorst–Pack scheme [19] was used, and convergence of energy and stress with respect to the mesh density was tested for each structure individually.

The WAl_2 structure calculations were performed on a 9 atom cell, and the *k*-point sampling was done with a $12 \times 12 \times 12$ Monkhorst–Pack grid, the $W_{14}Al_2$ structures with 16 atom cell and $12 \times 12 \times 12$ Monkhorst–Pack grid and the WAl_4 structure with a 30 atom cell and $8 \times 4 \times 8$ Monkhorst–Pack grid (convergence of energy to within 2.1×10^{-4} eV/atom, convergence of pressure to within 0.01 GPa). The ions were relaxed with the conjugate gradient method. The energy minimization procedure is iterative and proceeds until self-consistency within a prescribed tolerance of 10^{-6} eV per unit cell for electronic optimization and 10^{-4} eV per unit cell for ionic relaxation.

The electron localization function (ELF, η) was evaluated according to [20] with an ELF module already implemented within the VASP. ELF can be calculated in density functional theory from the excess kinetic energy density due to Pauli-repulsion, which is based on the Hartree–Fock pair probability of parallel spin electrons [20,21]. ELF is widely used to describe and visualize chemical bonding in crystalline structures, because it presents the understandable chemical bonding in direct space [22]. The value of ELF is scaled between 0 and 1. Initial structural input was taken from the experimental data.

3. Results and discussion

3.1. The crystal structure of WAl_2

Single crystals of WAl_2 were obtained as black hexagonal prisms with a metallic luster besides plate-like crystals of WAl_4 from the reaction mixture. The crystal structure was solved by direct methods, which yielded the position of the W atom position. The position of the Al atom was found by difference Fourier analysis. Experimental details of the structure analysis of WAl_2 are summarized in Table 1. The atomic coordinates and anisotropic displacement parameters (ADPs) are listed in Table 2, interatomic distances are given in Table 3.

WAl_2 crystallizes with the $CrSi_2$ structure type, which consists of edge and face sharing polyhedra. The W atom in the center of the polyhedron is coordinated by 10 Al atoms (Fig. 1). Four W atoms at bigger distances form the second coordination shell. The W–Al interatomic distances range from 2.604(4) to 2.778(4) Å, the W–W distance is 3.236(1) Å. The Al–Al distances vary between 2.572(2) and 2.779(4) Å, i.e. they are similar to the W–Al distances. These distances are comparable with the other known compounds of the W–Al system (Table 3). In WAl_4, the W–Al distances are in the range of 2.530–2.864 Å and the W–W distance is 3.311 Å [5]. The range of W–Al distances in WAl_5 is slightly

Table 1
Crystallographic data and structure refinement for WAl_2

Formula	WAl_2
Formula weight	237.81 g/mol
Temperature	295(2) K
Wavelength	0.71073 Å
Crystal system, space group	Hexagonal, $P6_422$ (181)
Unit cell dimensions	$a = 4.7422(1)$ Å
	$c = 6.6057(2)$ Å
Volume	128.65(1) Å^3
Z, calculated density	3, 9.208 g/cm^3
Absorption coefficient	67.761 mm^{-1}
Crystal size	$0.03 \times 0.03 \times 0.02$ mm^3
θ range	$4.96^\circ \leqslant \theta \leqslant 33.02^\circ$
Limiting indices	$-7 \leqslant h \leqslant 7$, $-7 \leqslant k \leqslant 7$, $-10 \leqslant l \leqslant 10$
Reflections collected/unique	4172, 169 [R(int) = 0.0408]
Refinement method	Full-matrix least-squares on F^2
Data/restraints/parameters	169/0/10
Goodness of fit on F^2	1.217
Final R indices [$I > 4\sigma(I)$]	$R_1 = 0.0226$, w$R_2 = 0.0512$
R indices (all data)	$R_1 = 0.0236$, w$R_2 = 0.0517$

Table 2
Atomic coordinates and anisotropic displacement parameters (10^4 Å^2) for WAl_2

Atom	Site	*x*	*y*	*z*
W	3*d*	1/2	1/2	1/6
Al	6*j*	0.8382(4)	0.1618(4)	1/6

Atom	U_{11}	U_{22}	U_{33}	U_{12}	U_{13}	U_{23}
W	83(3)	83(3)	130(3)	31(2)	0	0
Al	40(8)	40(8)	40(10)	2(1)	6(1)	6(1)

Table 3
Selected interatomic distances for WAl_2 and other known tungsten aluminides

	d (Å), WAl_2	*d* (Å), WAl_4 [5]	*d* (Å), WAl_5 [6]	*d* (Å), WAl_{12} [7]
W–Al	2.604(1)	2.48(14)–2.87(14)	2.75	2.72
	2.718(2)		2.83	
	2.778(4)			
W–W	3.236(1)	3.32(14)		
Al–Al	2.572(2)	2.53(14)–3.10(14)	2.75	2.79
	2.658(7)		2.83	2.88
	2.779(4)			

[1] In the atomic units, the unit of length is 1 Bohr = 0.529 Å.
[2] 1 eV = 1.602×10^{-19} J = 96.485 kJ/mol.

smaller, 2.75–2.83 Å [6] and only one W–Al distance is present in WAl_{12}, being 2.726 Å [7].

The compound WAl_2 is not listed in the phase diagram [8]. There are two postulated compounds with very close, but slightly different compositions, W_3Al_7 and W_7Al_{13}, which are proposed as high-temperature phases with stability areas of 1317–1345 °C for W_3Al_7 and 1336–1652 °C for W_7Al_{13}, respectively. Below 1302 °C, only a two-phase region with WAl_4 and a solid solution of Al in W being in equilibrium is given in the phase diagram. The present study gives strong hints that the phase diagram has to be revised in this region. WAl_4 and WAl_2 are in equilibrium at 1000 °C and a composition of W:Al = 1:3. This result is in contrast to the phase diagram. A DTA measurement of WAl_2 shows no thermal effects up to temperatures of 1500 °C, which is the limit of the used DTA apparatus.

Calculations concerning phase stability of WAl_2 have been performed with density functional theory. According to the phase diagram, WAl_2 should decompose into the WAl_4 and into the W (with 12.5% Al) phase [8]. In order to investigate the stability of the WAl_2 phase, calculations enabling the comparison of the enthalpy of WAl_2 with a mechanical mixture of the WAl_4 and W phase have been made.

For the tungsten rich side, several possibilities of the composition with 12.5% Al in the compound have been investigated in a $2 \times 2 \times 2$ supercell of *bcc* W (idealized $W_{14}Al_2$). The one with lowest energy proved to be the structure, where the alumina was in a nearest neighbour configuration. For the WAl_4, the structure from [5] was taken (Fig. 2). All structures have been fully relaxed at the given pressures. The enthalpy of the two stable phases have been calculated at relevant pressures and compared with the WAl_2 phase. Fig. 3 shows the enthalpy and volume of decomposition from WAl_2 into WAl_4 and $W_{14}Al_2$ as a function of pressure. The enthalpy of decomposition is negative below 29 GPa, i.e. at these pressures WAl_2 is not stable at 0 K when compared with the $W_{14}Al_2$–WAl_4 mixture. The difference volume of decomposition (averaged per atom) is based on the decomposition reaction $WAl_2 \rightarrow W_{14}Al_2 + WAl_4$. The difference is always positive, i.e. WAl_2 shows at all conditions a lower volume; hence, decomposition at high pressures cannot be expected. For none of the phases $W_{14}Al_2$ and WAl_4, a phase transitions at pressures within the investigated range, i.e. up to 35 GPa (see next paragraph), is reported. The results of the calculations may indicate that WAl_2 is indeed a high-temperature phase. At temperatures different from 0 K, entropic contributions to Gibb's energy $\Delta G = \Delta H - T\Delta S$ have to be considered. The entropy is given by $\Delta S = \gamma c_v \Delta V/V$ with γ the Grüneisen parameter, c_v the isochoric heat capacity, and $\Delta V/V$ the relative volume change. Unfortunately, γ and c_v are not known for this phase, but can be assumed as positive values. The relative volume change is also positive (volume difference 0.68 $Å^3$ per atom at 10^{-4} GPa), as obtained from the calculations. It follows that the entropic term is also positive. At high temperatures, therefore the entropic term becomes more dominant and lowers the value of ΔG, stabilizing WAl_2 as a high-temperature phase. The discrepancy with the experimental results can be explained by a sluggish kinetics or the kinetically hindered decomposition reaction.

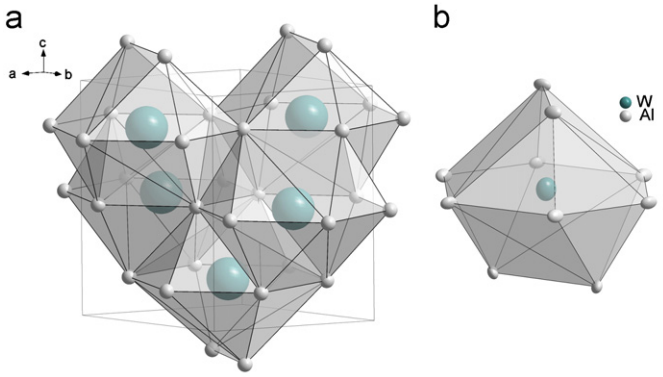

Fig. 1. (a) Perspective view of the crystal structure of WAl_2 ($CrSi_2$ structure type). It is built of polyhedra (b) that share common edges and faces. Ellipsoids are shown with 90% of probability.

3.2. High-pressure study

To confirm the results of the calculations and study the high-pressure behavior of WAl_2, X-ray powder diffraction measurements were done as a function of pressure using a DAC. Fig. 4 shows some representative powder diffraction patterns obtained from high-pressure measurements. Except the peak broadening, no drastic structural changes of the diffraction pattern were observed up to the highest reached pressure of 31.5(2) GPa in the experiments. After pressure release, the observed pattern is

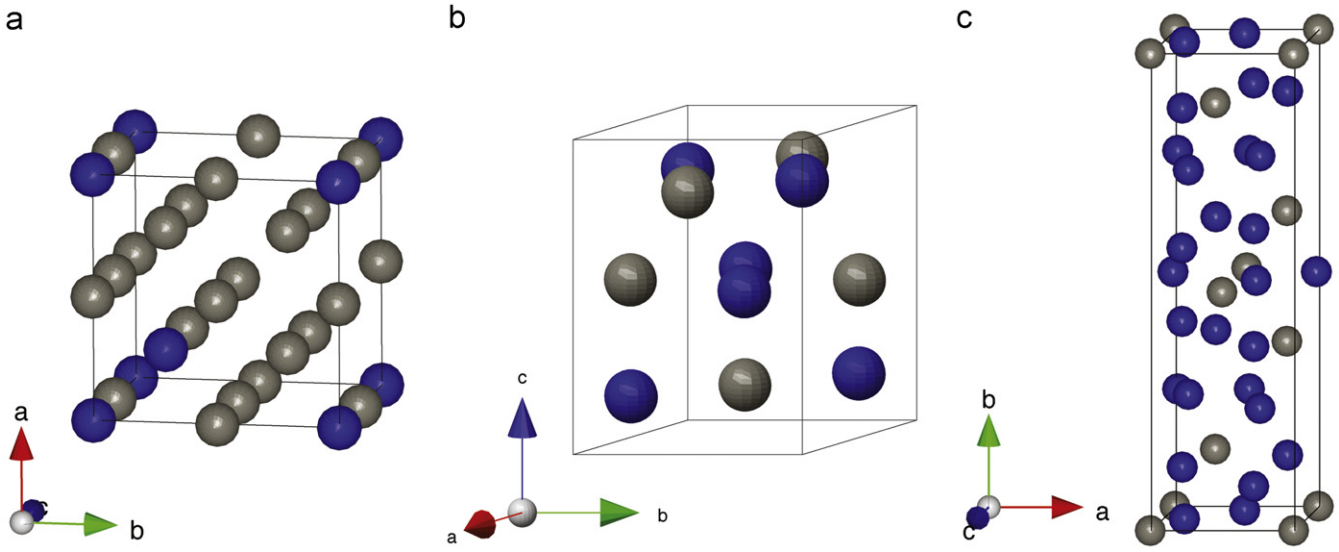

Fig. 2. (Color online) Unit cells of (a) W *bcc* with 12.5% Al impurities, (b) WAl_2 ($CrSi_2$ structure type), and (c) WAl_4. Al is denoted as dark blue and W as light gray spheres.

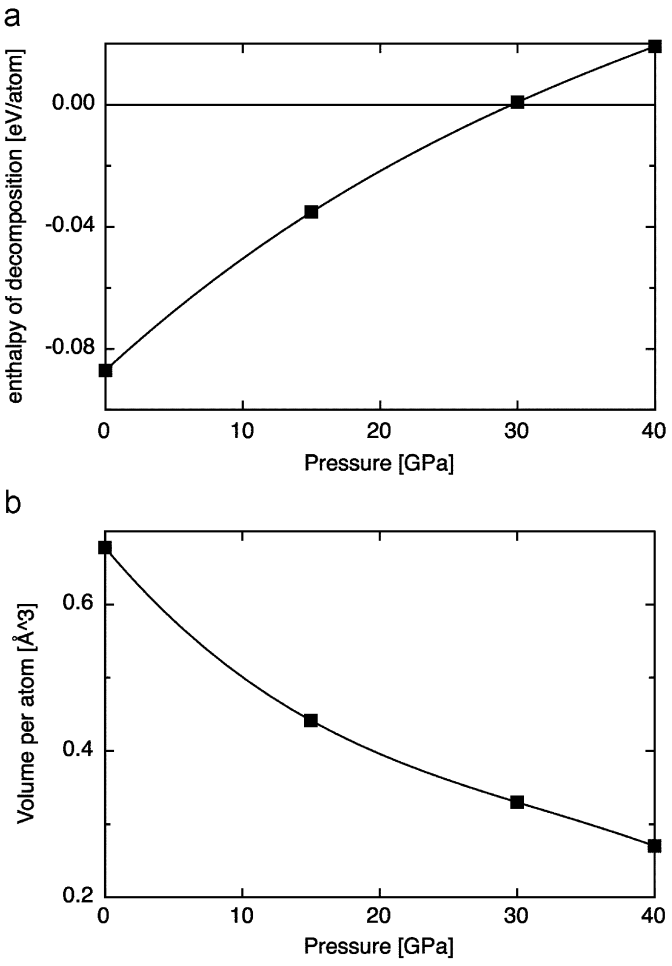

Fig. 3. Enthalpy (a) and volume (b) of decomposition based on the decomposition reaction $WAl_2 \rightarrow W_{14}Al_2+WAl_4$.

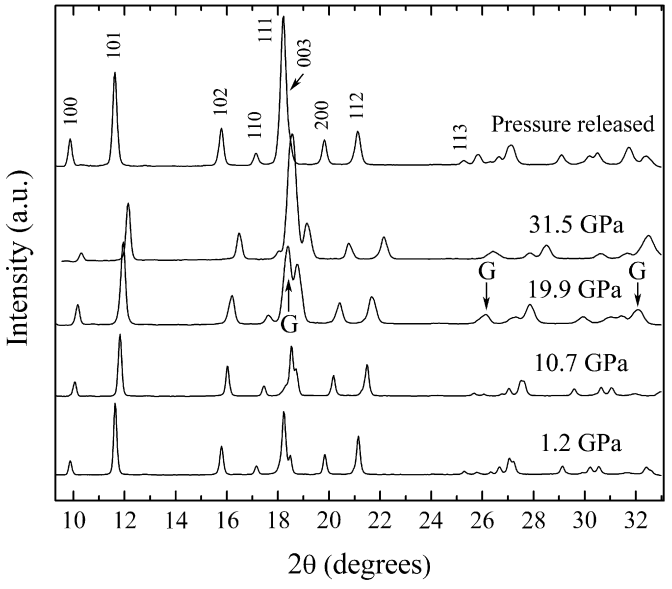

Fig. 4. Selected X-ray powder diffraction patterns at different pressure. G indicates diffraction peaks from the W gasket.

comparable to that collected before the high-pressure study. The lattice parameters and structures were refined based on the WAl_2 structure using the Rietveld method. A typical Rietveld refinement

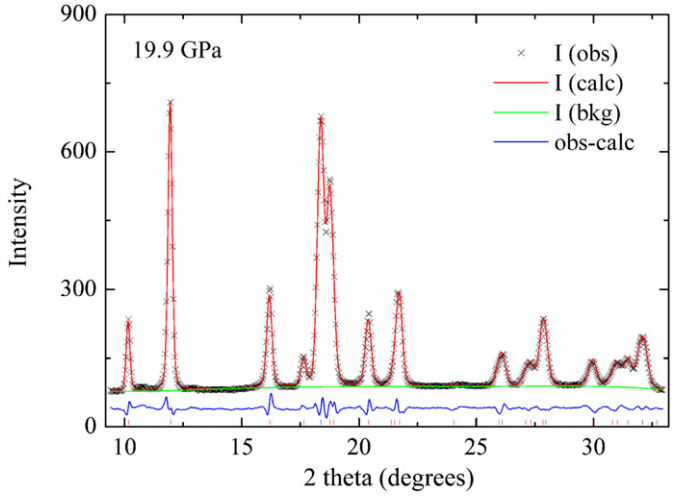

Fig. 5. (Color online) A typical Rietveld refinement of a powder diffraction pattern of WAl_2 collected at 19.9 GPa.

Table 4
Experimental and calculated lattice parameters and unit-cell volume of WAl_2 as a function of pressure

Experimental				Calculated			
P (GPa)	a (Å)	c (Å)	V (Å^3)	P (GPa)	a (Å)	c (Å)	V (Å^3)
1.2(1)	4.752(1)	6.622(1)	129.51(6)	10^{-4}	4.869	6.795	139.52
2.7(2)	4.737(1)	6.603(2)	128.30(11)	5	4.815	6.743	135.38
3.8(2)	4.727(1)	6.592(1)	127.55(8)	10	4.768	6.696	131.81
5.2(4)	4.716(2)	6.579(2)	126.74(13)	15	4.727	6.652	128.70
7.4(6)	4.700(1)	6.563(2)	125.56(9)	20	4.689	6.611	125.89
9.1(3)	4.685(1)	6.546(3)	124.42(12)	25	4.655	6.573	123.36
10.7(2)	4.674(2)	6.536(2)	123.65(15)	30	4.623	6.539	121.03
11.2(1)	4.670(1)	6.532(3)	123.36(12)	40	4.565	6.477	116.90
12.3(2)	4.667(2)	6.523(2)	123.03(16)				
13.1(3)	4.659(1)	6.517(1)	122.53(5)				
13.3(4)	4.657(1)	6.516(2)	122.39(9)				
14.5(2)	4.650(3)	6.514(3)	121.98(21)				
15.9(3)	4.643(1)	6.503(1)	121.39(9)				
19.6(4)	4.616(2)	6.466(2)	119.32(14)				
19.9(6)	4.621(2)	6.478(2)	119.82(12)				
23.2(1)	4.605(1)	6.450(2)	118.46(8)				
27.0(1)	4.588(2)	6.430(3)	117.24(14)				
31.5(3)	4.565(2)	6.404(4)	115.58(17)				

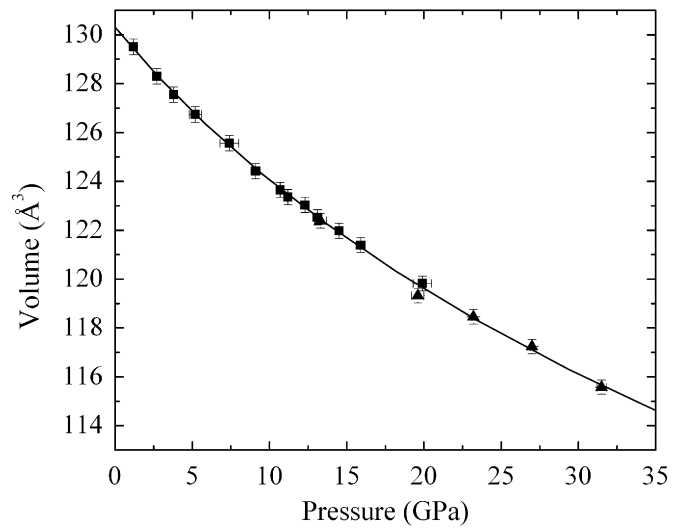

Fig. 6. Unit-cell volume of WAl_2 as a function of pressure. The solid line corresponds to a third-order Birch–Murnaghan equation of state. The square and triangle symbols represent two different loadings.

of WAl_2 at high pressure is shown in Fig. 5. The structure was therefore stable within the framework of the high-pressure experiment. The obtained lattice parameters as a function of pressure are listed in Table 4. A third-order Birch–Murnaghan equation of state was fitted to the experimental data (Fig. 6). The bulk modulus of WAl_2 was determined as $K_0 = 168(11)$ GPa and its pressure derivative $K' = 7.7(1.0)$. It was found that the compressibility along the *a*-direction is higher than along the *c*-direction (Fig. 7). This can be understood as within the polyhedra, the W–Al distances in the *a*–*b*-plane are larger (2.718(2) Å) than the corresponding distances out of this plane (2.6036(9) Å).

To prove the experimental results, the volume as a function of pressure was calculated by using VASP. In Table 4, the obtained values for the lattice parameters are given. Due to the applied GGA method, the calculated volume is overestimated. Fitting a third-order Birch–Murnaghan equation of state to the pressure volume data yields a $K_0 = 157.2(8)$ GPa and $K' = 4.16(6)$. The experimental and calculated bulk moduli are within the experimental errors. Their pressure derivatives differ significantly. A possible explanation of the deviation could be strain, induced by the increasing nonhydrostaticity of the pressure medium with increasing pressure.

The value of the bulk modulus is comparable to other compounds containing Al and heavy transition metals in comparable ratios (see e.g. [2] and references therein). The recently revisited $CuAl_2$ [23] shows a lower value of $K_0 = 117(13)$ GPa, which could possibly be related to the lower electron concentration of the transition metal.

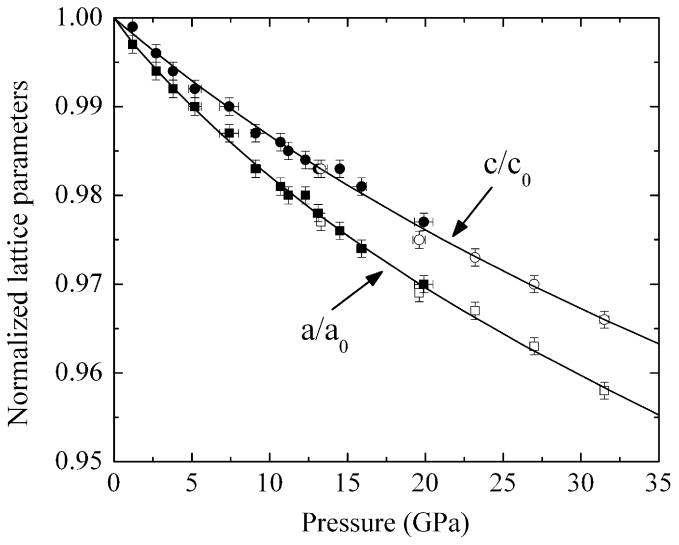

Fig. 7. Normalized lattice parameters of WAl_2 as a function of pressure. The solid line represents a third-order Birch–Murnaghan equation of state fit to the dataset. The solid and empty symbols indicate two different loadings.

3.3. Chemical bonding

In order to get a deeper understanding of the structure of WAl_2, we analyzed the chemical bonding by means of the ELF. A topological analysis of the ELF shows that the maxima of ELF (attractors) are located in a plane formed by two W and two Al atoms (Fig. 8a and b). This basin is (2Al+2W)-tetrasynaptic, which means it has common borders with two core basins of Al and two core basins of W, respectively. They are located in the middle of the short Al–Al contacts (2.572(2) Å). Similar to the observation in $CuAl_2$ [23], for which a (2Al+2Cu)-tetrasynaptic basin was observed, a (2Al+2W)-tetrasynaptic basin is present in WAl_2. The attractor can be interpreted as a four-center bond of two W and two Al atoms. There are also smaller maxima of ELF present, which are located between W and Al atoms in the (001) planes. These maxima are biased towards the Al atoms. Correlating to the two different W–Al distances present in the plane, at shorter W–Al distances, these are slightly more pronounced than at the longer distances (Fig. 8d). These attractors indicate amounts of covalent interactions between the W and Al atoms. Visualization with a lower isosurface value of $\eta = 0.53$ shows an ELF topology of typical metallic systems which present large areas of nearly constant electron localization close to the jellium value 0.5 [24]

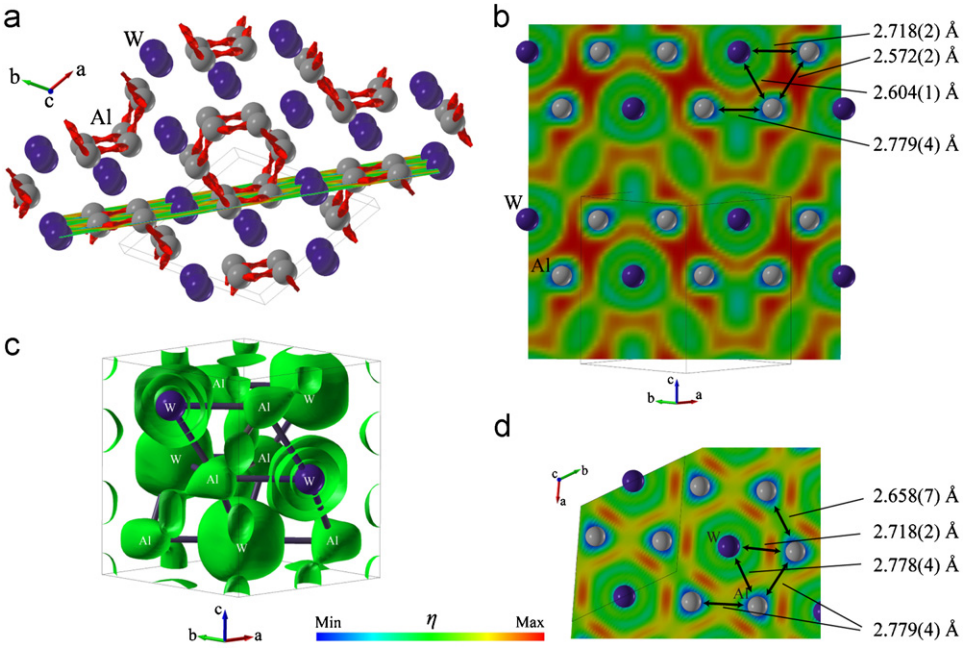

Fig. 8. (Color online) Electron localization function (ELF η) for WAl_2: (a) isosurface of $\eta = 0.75$; (b) 2D cross-section through W and Al atoms parallel to the (110) plane; (c) isosurface of $\eta = 0.53$; (d) 2D cross-section through W and Al atoms parallel to the (001) plane.

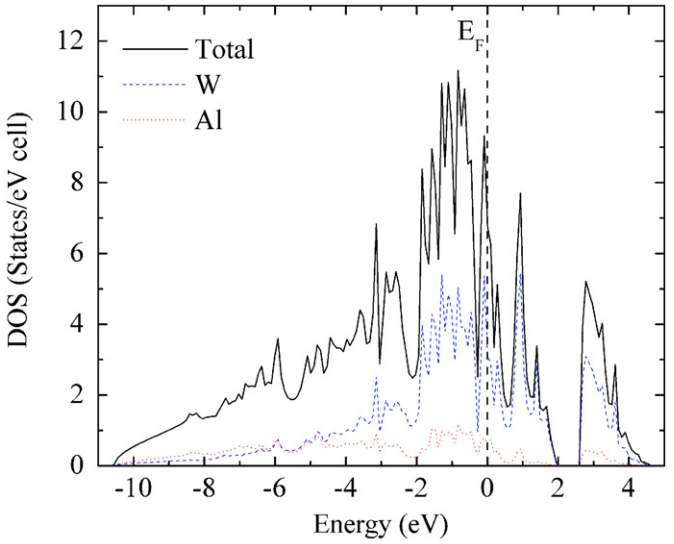

Fig. 9. (Color online) Electronic density of states for WAl_2. The solid line represents the total DOS, contributions of W and Al are shown as dotted (red) and dashed lines (blue).

(Fig. 8c). The presence of the different bonding in the *a*- and *b*-plane and perpendicular to it, i.e. a four center-bond and the weaker attractors found in the (001) planes explain very well the anisotropic compression behavior of WAl_2.

The partial electronic density of states (DOS) indicates that W and Al atoms contribute to the DOS at the Fermi energy (Fig. 9). WAl_2 is a metal, the calculated DOS shows a local maximum at the Fermi level. Please note that the partial DOS does not sum up to the total DOS, as it only covers the states projected on to the atoms.

4. Conclusions

The intermetallic compound WAl_2 was first characterized by single-crystal X-ray diffraction, its bonding by means of the ELF. This compound is the first aluminide crystallizing with the $CrSi_2$ structure type. The structure was found to be stable up to about 31.5 GPa within the framework of the experiment. ELF revealed the presence of a four-center bond and partial covalent W–Al bonding. The bonding nicely explains the anisotropic compression behavior of the compound. Quantum chemical calculations strongly indicate that WAl_2 is a high-temperature phase, which could not have been proven experimentally. With respect to the proposed high-temperature phases in the W–Al system, the present work gives strong indications that the phases proposed as W_3Al_7 and W_7Al_{13} are in fact WAl_2 and the phase diagram should be reinvestigated in detail.

Acknowledgment

This work was supported by the Swiss National Science Foundation (SNF) under Grant no. 200021-115871.

Appendix A. Supplementary data

Supplementary data associated with this article can be found in the online version at doi:10.1016/j.jssc.2008.06.053.

References

[1] K. Urban, M. Feuerbacher, J. Non-Cryst. Solids 334 and 335 (2004) 143.
[2] G. Krauss, Q.F. Gu, S. Katrych, W. Steurer, J. Phys.-Condens. Matter 19 (2007) 116203.
[3] Q.F. Gu, G. Krauss, Y. Grin, W. Steurer, J. Solid State Chem. 180 (2007) 940.
[4] G. Krauss, Q.F. Gu, J. Solid State Chem., in press, 2008, doi:10.1016/j.jssc.2008.04.031.
[5] J.A. Bland, D. Clark, Acta Crystallogr. 11 (1958) 231.
[6] J. Adam, J.B. Rich, Acta Crystallogr. 8 (1955) 349.
[7] J. Adam, J.B. Rich, Acta Crystallogr. 7 (1954) 813.
[8] Pauling File Binaries Edition, Version 1.0, 2002.
[9] M. Feuerbacher, C. Thomas, J.P.A. Makongo, et al., Z. Kristallogr. 222 (2007) 259.
[10] Oxford Diffraction Ltd. XCalibur, CrysAlis Software System, Version 171.32.5, 2007.
[11] G.M. Sheldrick, Program SHELX-97 for Crystal Structure Determination, University of Goettingen, 1997.
[12] A.P. Hammersley, S.O. Svensson, M. Hanfland, A.N. Fitch, D. Häusermann, High Press. Res. 14 (1996) 235.
[13] A.C. Larson, R.B. Von Dreele, LANSCE, MS-H805, Los Alamos National Laboratory, Los Alamos, NM 87545.
[14] R.J. Angel, Rev. Min. Geochem. 41 (2000) 35.
[15] G. Kresse, J. Furthmuller, Comput. Mater. Sci. 6 (1996) 15.
[16] G. Kresse, J. Furthmuller, Phys. Rev. B 54 (1996) 11169.
[18] P.E. Blochl, Phys. Rev. B 50 (1994) 17953.
[17] J.P. Perdew, K. Burke, M. Ernzerhof, Phys. Rev. Lett. 77 (18) (1996) 3865.
[19] H.J. Monkhorst, J.D. Pack, Phys. Rev. B 13 (1976) 5188.
[20] A. Savin, H.J. Flad, J. Flad, H. Preuss, H.G. von Schnering, Angew. Chem. Int. Ed. Engl. 31 (1992) 185.
[21] M. Kohout, K. Pernal, F.R. Wagner, Y. Grin, Theor. Chem. Acc. 112 (2004) 453.
[22] ELF website: 〈http://www.cpfs.mpg.de/ELF〉.
[23] Y. Grin, F.R. Wagner, M. Armbrüster, M. Kohout, A. Leithe-Jasper, U. Schwarz, U. Wedig, H.G. Von Schnering, J. Solid State Chem. 179 (2006).
[24] C. Gatti, Z. Kristallogr. 220 (2005) 399.